




TECHNICAL ARTICLE

Microstructure, Mechanical and Tribological Properties of the x SiC— $(1-x)$ WC—10 wt.% Co Composites Prepared by High-Energy Milling and Spark Plasma Sintering

HEYTOR V.S.B. AZEVEDO ^{1,2,3,8} RAFAEL A. RAIMUNDO,⁴
LUÍS M.F. MORAIS,⁵ MURILLO M.B.M. JUNIOR,¹ LUCAS P.P. BARRETO,⁶
DANIELLE G.L. CAVALCANTE,² MARCELLO FILGUEIRA,⁷
and UÍLAME U. GOMES¹

1.—Graduate Program in Materials Science and Engineering, Federal University of Rio Grande do Norte, Natal 59078-970, Brazil. 2.—Graduate Program in Mechanical Engineering, Federal University of Paraíba, João Pessoa 58051-900, Brazil. 3.—Federal Institute of Education, Science and Technology of Rio Grande do Norte, IFRN, Mossoró 59628-330, Brazil. 4.—Department of Physics, UFPB, João Pessoa 58051-900, Brazil. 5.—Graduate Program in Mechanical Engineering, Federal University of Rio Grande do Norte, Natal 59078-970, Brazil. 6.—Graduate Program in Chemical Engineering, Federal University of Rio Grande do Norte, Natal 59078-970, Brazil. 7.—Centre of Science and Technology, Laboratory of Advanced Materials, Northern Fluminense State University, Campos dos Goytacazes 28013-602, Brazil. 8.—e-mail: heytorazevedo@hotmail.com

This work proposes to characterize the composites manufactured of SiC, WC, and Co [x SiC— $(1-x)$ WC—10 wt.% Co], with $x = 0, 0.25, 0.50, 0.75$ and 1. These composites were prepared by high-energy milling (HEM) and consolidated by spark plasma sintering (SPS). The results showed that HEM promoted a decrease in particle size, dispersion, and homogenization of the constituent phases, improving the densification and mechanical properties of the composites. The WC-Co showed high relative density (96.37%) and microhardness (9.4 GPa) values. The tribological behavior of the composites was evaluated by a pin-on-disk tribometer, applied against 1020 steel discs with a 5-N load in non-lubricated conditions. There was a significant effect from the variations in the contents of SiC and WC in the wear volumes (3.13×10^{-2} – 49.0×10^{-2} mm³) and wear rates (0.63×10^{-5} – 9.83×10^{-5} mm³/N m) of the composites. Tribological tests showed that the composites sintered by SPS proved to be a promising material with good tribological performance and attractive for components/devices subjected to wear.

INTRODUCTION

Silicon carbide (SiC) is a ceramic material, artificially produced by mixing stoichiometric proportion of silica sand (silica) and petroleum coke. It has a set of special physical–chemical properties, such as high hardness and mechanical stability at high temperatures, excellent thermal conductivity, low coefficient of thermal expansion, excellent wear resistance, and high resistance to corrosion and

oxidation, among others.^{1–4} This low-density, high-temperature ceramic is present in various industrial applications where tribological conditions are required, such as cylinder liners, cutting tools, abrasive machining, brakes, valves, etc.^{5–7} SiC ceramics and their composites have been widely studied by researchers in different wear conditions, due to their excellent wear resistance.^{8–10}

WC-Co-based cermets play an important role in the manufacturing processes of cutting tools due to their suitable mechanical properties such as hardness and toughness.¹¹ In this context, several researchers have sought improvements in the mechanical properties of WC-Co-based cermets

(Received May 22, 2022; accepted February 21, 2023; published online March 14, 2023)

through the incorporation of a second ceramic phase.^{12–14} The ZrO₂ ceramic has been widely studied for a WC replacement in cemented carbide WC-Co, because, according to Lin et al.¹⁵ it notably improves the flexural strength and impact strength of WC-20 wt.%Co composites with added ZrO₂ (3Y), but the hardness values have changed little. Other elements, such as VC and cBN, have also been frequently studied, and, according to research by Zhenhua et al.¹⁶ the results showed that the relative density, Vickers hardness, and fracture toughness of WC-based carbide materials decreased significantly as the cBN and VC contents increased.

Siwak and Garbiec¹⁷ improved the hardness of WC-Co cermets with the addition of Cr₃C₂ and TaC grain growth inhibitors, sintered by spark plasma. Olubambi et al.¹⁸ investigated the influence of mixed binder additives based on cobalt and zirconia on the mechanical properties and tribological characteristics of WC-based spark plasma-sintered cermet composites. Fazili et al.¹² studied the effect of the addition of Al₂O₃ on the electrochemical and mechanical properties of WC-Co-Al₂O₃ composites, using spark plasma sintering (SPS). Genga et al.¹⁹ evaluated the effect of the grain size of NbC additions on the microstructure and mechanical properties of WC-NbC-Co cermets sintered by pulsed electric current sintering. Lee et al.²⁰ investigated the microstructure and mechanical properties of carbides cemented with WC-TiC-Co manufactured by sintering with a hot isostatic pressing process. Recently, we have studied the microstructural, mechanical, and tribological properties of Al₂O₃-WC-Co composites processed by high-energy milling (HEM) and consolidated by SPS.²¹ The results showed that the manufactured composites are promising materials for abrasive machining applications, once the mechanical and tribological properties of Al₂O₃ have been improved by the addition of WC-Co. Thus, the effect of adding SiC to WC-Co cermets with a variation of the carbide contents (SiC, WC), together with a complete analysis of the mechanical and tribological properties of the composites [x SiC—(1- x) WC—10 wt.% Co], where $x = 0, 0.25, 0.50, 0.75, \text{ and } 1$, have not yet been investigated in the literature.

SPS is an innovative technique for consolidating materials. It provides adequate conditions to produce a wide variety of materials with high densification, due to its exclusive advantages of applying pressure at high temperatures, heat treatments with a Joule effect, high heating rates, and vacuum conditions.^{22,23} This technique has the ability to quickly sinter materials that are difficult to sinter at lower temperatures, leading to better final properties thanks to better control of the microstructure,²⁴ while conventional sintering methods lead to numerous problems, such as low heating rate and long periods to reach high temperatures.^{25,26} In addition, the thermal cycle is shorter, leading to energy savings per unit of material produced.²⁷

The HEM technique is increasingly becoming more common for mixing and homogenizing fragile ductile systems (ductile component Co, fragile SiC and WC), since this way of milling transfers energy to the particles, causing deformation, shape control, dispersion, and comminution of these components.^{28,29} Câmara et al.³⁰ successfully utilized HEM to promote the mixture and homogenization of the Cu-SiC system. Silva et al.³¹ successfully obtained the interaction of the WC-Al₂O₃ system through humid HEM using ethyl alcohol and 400 rpm rotation speed. Consecutively, the sintering stage of composite powders generally follows the HEM. Therefore, SPS is a widely utilized technique to sinter systems of difficult consolidation with a short time and good efficiency, compared with conventional sintering, such as SiC-WC, SiC-WC-Co, TiC-SiC-WC, and ZrB₂-SiC-WC^{32–34} composite materials.

In the present work, composite powders of x SiC—(1- x) WC—10 wt.% Co, with $x = 0, 0.25, 0.50, 0.75, \text{ and } 1$, were processed by HEM for up to 30 h. The SPS technique was adopted for the consolidation of the composite powders. Based on the experiments and the results, the influence of HEM on the mechanical and tribological properties of the composites has been discussed in order to evaluate potential applications for components/devices subjected to wear, such as applications in cylinder liners, abrasive machining, cutting tools, valves, etc.

EXPERIMENTAL

Commercial silicon carbide (Saint-Gobain, Brazil), tungsten carbide (Lainez, Brazil), and cobalt (Stark, Germany) powders were used as precursor materials. All the powders were 99.9% pure. Several mixtures were obtained containing x SiC—(1- x) WC—10 wt.% Co, with x values of 0, 0.25, 0.50, 0.75, and 1. Five composites were produced, in which the variation of SiC and WC represent 90% weight in each composition, while the cobalt concentration of 10% weight remained unchanged, thus resulting in a representative study of the carbide contents.

The composite powders of each mixture were subjected to HEM using a crucible and carbide balls. The ball-to-powder mass ratio was fixed at 5:1, and the total powder mass was 20 g. The composite powders were milled in a planetary mill (Puvri-sette 6; Fritsch) for up to 30 h in the presence of 20 mL of ethyl alcohol at a grinding speed of 400 rpm. According to the work developed by Liu et al.³⁵ and Raimundo et al.³⁶ in ductile-fragile systems, the ideal time for processing these systems by HEM is 30 h. For that reason, this time was adopted in this work. The materials were consolidated by SPS (Dr. Sinter. Lab. Jr. SPS-211 LX; Kagaku). Powders of each composition were placed in a graphitic cylindrical matrix. Sintering started with the evacuation of the system and then a

uniaxial mechanical pressure of 40 MPa was applied. Next, a pulsating current was activated and maintained at 1650 °C with a heating rate of 65 °C/min, remaining for 5 min and then being switched off. At the end of the process, the specimens were cooled to room temperature. The sintering process was carried out under a vacuum of 100 Pa. Three specimens were obtained in a single sintering step for each composition.

Phases in the composites were identified by x-ray diffraction (XRD; Miniflex II; Rigaku). The following parameters were used: angular variation from 30 to 90°, speed of 3° per min, and step of 0.02. The effect of HEM on the morphology of the starting and composite powders was investigated by field-emission scanning electron microscopy (FESEM; Auriga; Zeiss). Particle size distribution of the powders was evaluated in the ImageJ software by measuring the size of 200 particles in each specimen.³⁷ The microstructure of the sintered composites was investigated by scanning electron microscopy (SEM; TM3000; Hitachi).

The apparent density of the sintered specimens was measured using an immersion method in distilled water at room temperature and atmospheric pressure, according to the Archimedes principle (standard: ASTM B962-13).³⁸ Hence, the relative density of the sintered specimens was calculated from the correlation between the theoretical density and the apparent density, as discussed in other works.^{39,40} The Vickers microhardness of the specimens was determined using an indentation technique. The indentation tests were performed on the surface of the specimens by a digital microhardness tester (MV2000A; Pantec) under a load of 9.807 N for 10 s at room temperature, according to standard ASTM E384-99.⁴¹ Each test was replicated eight times and the mean value was reported.

Before sliding tests, 1020 steel discs were sanded to reduce surface roughness in wear behavior, using 200–1200-mesh sandpaper. A total of 1020 steel discs were kept at a contact sliding speed of 0.5 m/s and a disc rotation of 500 rpm. Sliding tests were performed on a pin-on-disk tribometer (TE-165LE; Magnum Engineers India) in non-lubricated conditions. The composite powders were sintered into stationary pins (5 mm in diameter) and a load of 5 N was applied during the test.

Sliding tests were performed at room temperature with the relative humidity ranging from 40 to 60%. The tribological tests on each sample were performed under the same conditions with a sliding duration of 30 min (or 942 m distance). The friction force was recorded continuously using an electronic sensor to generate a coefficient of friction (COF) in real time.

Surface roughness analysis by optical profilometry was carried out before and after the tribological tests, using a CCI MP Taylor Hobson® profilometer. The results were analyzed using the

MountainsMap® software. These analyses made possible the characterization of the specimen's surface conditions before and after the sliding wear tests through the non-contact 3D measurement method, using magnifications of $\times 50$, with a resolution of 512×512 pixels. The topography of the surface was acquired by combining several measurements.

The loss of wear mass was characterized by an electronic scale (AUW220D; Shimadzu) with a resolution of 0.1 mg. Evaluation of the specific wear rate is usually calculated by measuring the wear volume (V) through the loss of mass (ΔW) that occurred after the test (Eq. 1) and applying it to the equation developed by Archard (Eq. 2):⁴²

$$V = \frac{\Delta W}{\rho c} = \frac{W_i - W_f}{\rho c} \quad (1)$$

$$K = \frac{V}{F \cdot S} \quad (2)$$

The loss of mass of the samples (ΔW) is obtained by the difference between the initial (W_i) and the final (W_f) masses of the specimens. The specific wear rate indicator is K (mm^3/Nm), the volume of worn material is V (mm^3), the test load is F (N), and S is the sliding distance (m). The wear volume, V , is correlated with the loss of mass after the test and the specific mass of the composite (ρc).

RESULTS AND DISCUSSION

Morphological Characterization of the Precursor Powders

Figure 1 shows the FESEM results and particle size distribution for the SiC, WC, and Co powders. The SiC powder exhibited a faceted morphology with sharp edges and homogeneity with the average particle size distribution of $34.76 \mu\text{m}$, as seen in Fig. 1a, b. The WC powder exhibited particles with irregular morphology and an average size distribution of $0.278 \mu\text{m}$ (Fig. 1c, d). The Co powder had a spherical shape and the presence of small particles adhered to the surface of larger particles (Fig. 1e). Particle agglomeration was also observed with an average particle size distribution of $3.25 \mu\text{m}$ (Fig. 1f).

Effect of High Energy Milling on the Morphology of Composite Powders

Figure 2a–e shows FESEM micrographs of the composite powders ground for 30 h. The starting powders are well dispersed, showing that the HEM promoted particle size reduction, homogenization and dispersion of the specimen's constituent phases. In the grinding process, the powders were subjected to high-energy collisions, which cause plastic deformation, cold welding, and dust fracture. The most fragile ceramic particles (SiC, WC) suffered

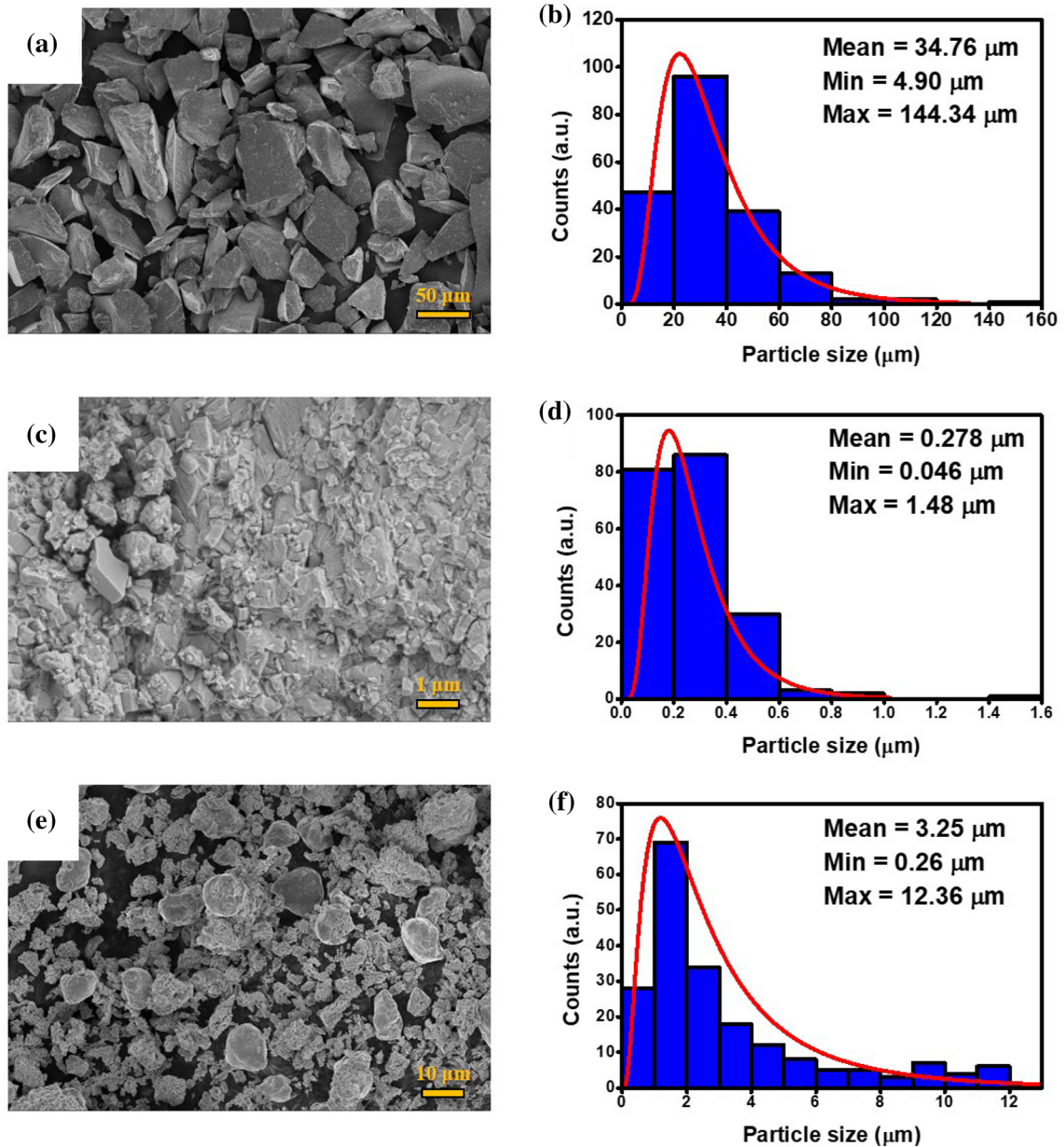


Fig. 1. FESEM micrographs and particle size distribution of the starting powders: (a, b) SiC, (c, d) WC, and (e, f) Co.

fracture, were refined, and were welded in the ductile matrix (Co).

Figure 3 shows the average particle size distribution of the composite powders ground for 30 h. As shown, the average particle size distribution (258 nm) was greater for the SiC-Co composition ($x = 1$). As the SiC content decreased and the WC increased in the composite powders, the average particle size distribution gradually decreased, $x = 0.75$ (155 nm), $x = 0.50$ (116 nm), and $x = 0.25$ (83 nm). This decay trend is possibly related to the carbide particle sizes (SiC, WC) in the composition of the specimens, since the SiC and WC ceramics have the larger and the smaller granulometry, respectively, as shown in Fig. 1. The lowest average

particle size distribution (62 nm) was confirmed for the WC-Co composite ($x = 0$).

Structural Characterization of the Composite Powders

Figure 4 shows XRD patterns of the composite powders [x SiC—(1- x) WC—10 wt.% Co] obtained by HEM. The peaks observed in the x-ray patterns are characteristic of WC [WC-type structure, with lattice parameters $a = b = 2.9062$ Å and $c = 2.8377$ Å, space group P-6m2 (187)],⁴³ SiC [lattice parameters $a = b = 3,078$ Å and $c = 143.52$ Å, ICSD No. 23887, space group R 3 m H (160)],⁴⁴ and Co (hcp#Mg-type structure, with lattice parameters $a = b = 2.5054$ Å and $c = 4.0893$ Å, ICSD No. 44990, space group P63/

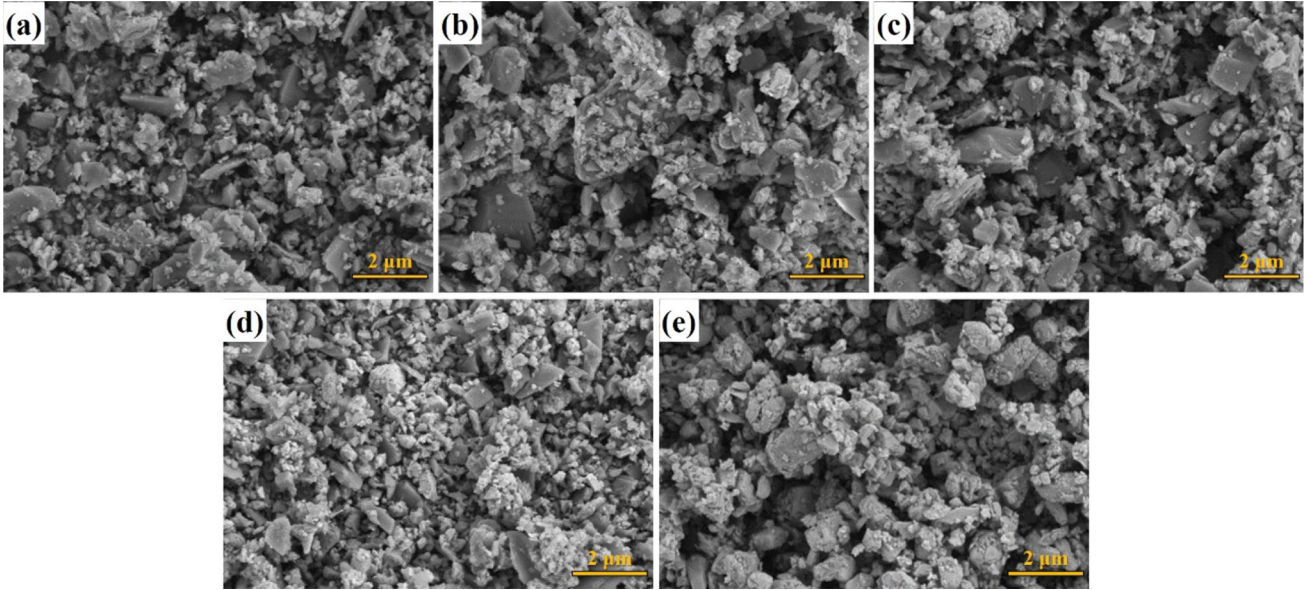


Fig. 2. FESEM micrographs of the x SiC–(1- x) WC–10 wt.% Co composite powders ground for 30 h: (a) $x = 1$, (b) $x = 0.75$, (c) $x = 0.50$, (d) $x = 0.25$, and (e) $x = 0$.

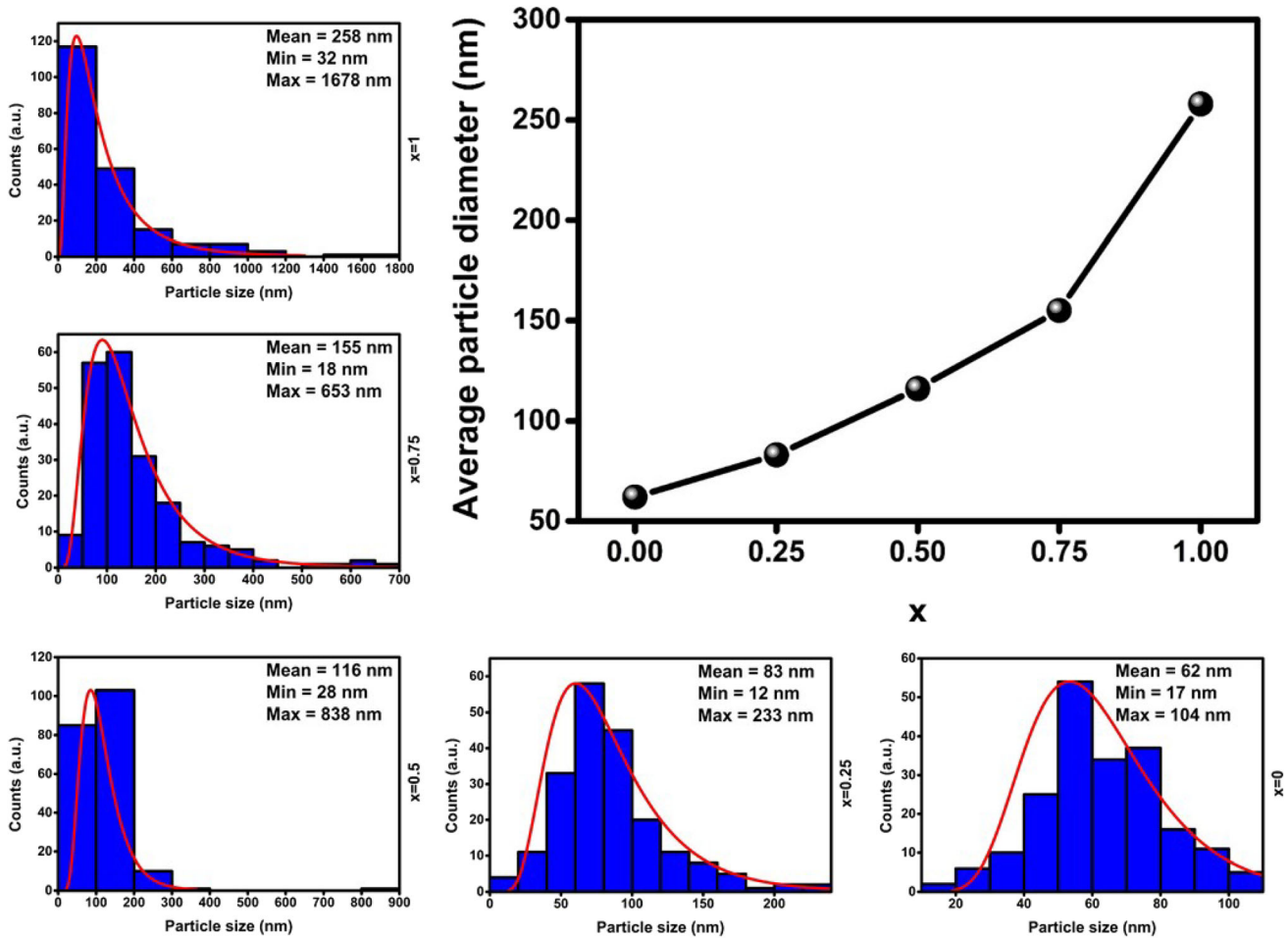


Fig. 3. Particle size distribution of the x SiC–(1- x) WC–10 wt.% Co composite powders ground for 30 h.

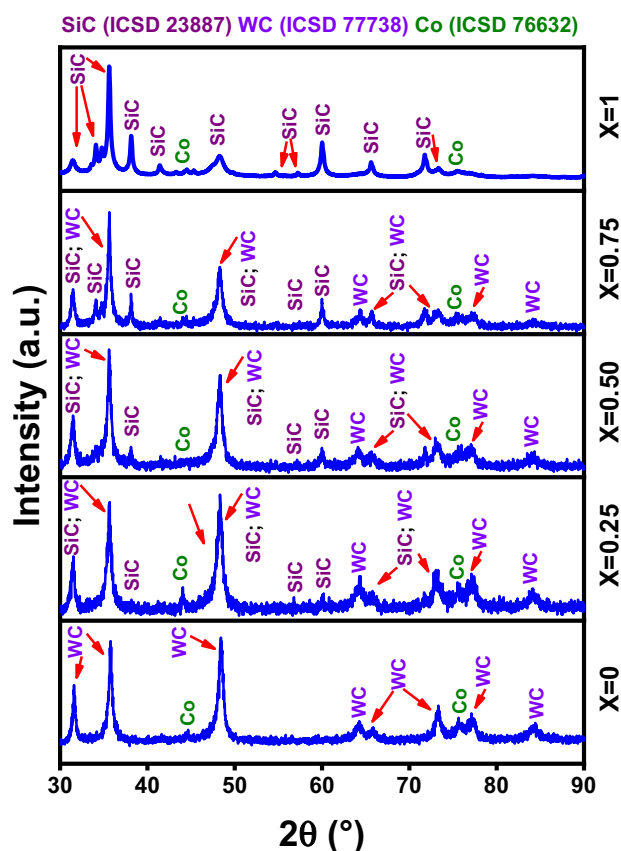


Fig. 4. XRD patterns of the x SiC—(1- x) WC—10 wt.% Co composite powders ground for 30 h.

mmc (194)].⁴⁵ The WC phase has eight peaks located at positions $2\theta = (31.6^\circ, 35.8^\circ, 48.4^\circ, 64.2^\circ, 65.8^\circ, 73.3^\circ, 77.1^\circ, \text{ and } 84.4^\circ)$ which are indexed to the Miller planes (001), (100), (101), (110), (002), (111), (102), and (021), respectively. For SiC, a series of diffraction peaks can be seen, while the Co peaks are detected at positions $2\theta = (44.06^\circ \text{ and } 75.64^\circ)$ and are indexed to the Miller planes (002) and (110), respectively.

Structural Characterization of the Sintered Composite

Figure 5 shows the XRD patterns of x SiC—(1- x) WC—10 wt.% Co sintered specimens prepared with precursor powders ground for 30 h. Only the WC, SiC, and Co peaks were identified. There is no evidence of secondary phases from the reactions of the WC, SiC, and Co phases during the sintering. All the peaks are identical in position (2θ) when compared to the ground powders. They also present full widths at half-maximum which were decreased when compared to the composite powders. This indicates an increase in the size of the phase crystallites. Phase C [graphite (2H)]#C-type structure, with lattice parameters $a = b = 2.46 \text{ \AA}$ and $c = 6.71 \text{ \AA}$, ICSD No. 76767, space group P 63/mmc (194)] was identified in position $2\theta = 54.59^\circ$ and is

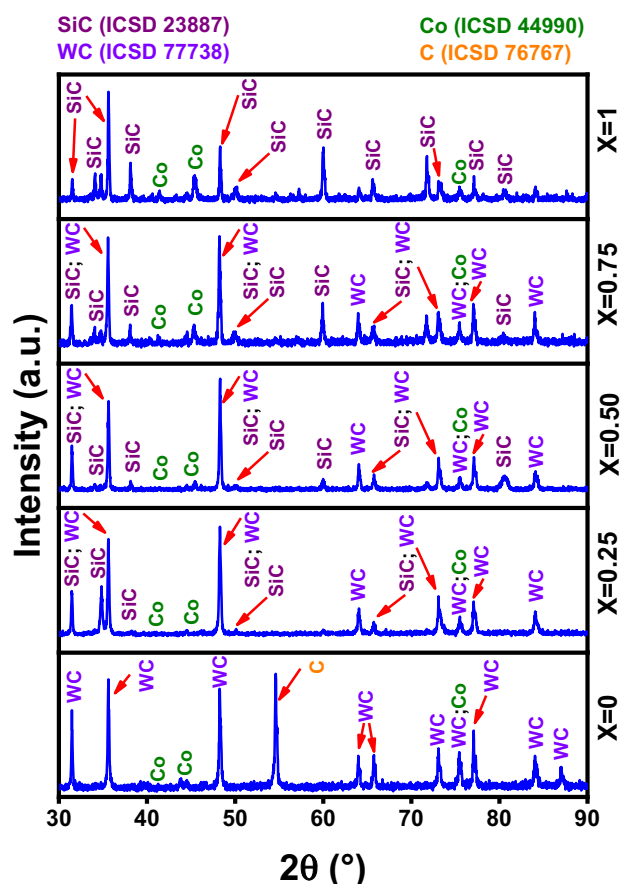


Fig. 5. X-ray diffraction patterns of the x SiC—(1- x) WC—10 wt.% Co composites prepared with the composite powders ground for 30 h and subject to SPS at 1650°C .

indexed to the Miller plane (004). This phase comes from the mold matrix of the SPS process.

Microstructure of Sintered Composites

SEM images of the sintered samples derived from the powders milled for 30 h are shown in Fig. 6. In Fig. 6a, it is possible to perceive the presence of dark SiC grains, while the Co grains are lighter in color. Figure 6b represents the microstructure of the composite $x = 0.75$, and reveals the beginning of the presence of WC, even in small amounts. Figure 6c, d increasingly shows the presence of WC in the composites, corroborating their increase in weight content. Prismatic-shaped WC grains are seen in Fig. 6e. In fact, according to García et al.,⁴⁶ in sintered cemented carbides (WC-Co) the WC phase can be recognized as prismatic grains in the microstructure. As can be seen, the increase in milling time allowed homogenization, dispersion, and uniform distribution of ceramic particles (SiC, WC) in the Co metallic matrix. Another important aspect is the limitation of grain growth provided by SPS, due to the short residence time associated with the high heating rate. The micrographs show a dense compact with a microstructure free of microcracks, with the SiC and WC grains interconnected

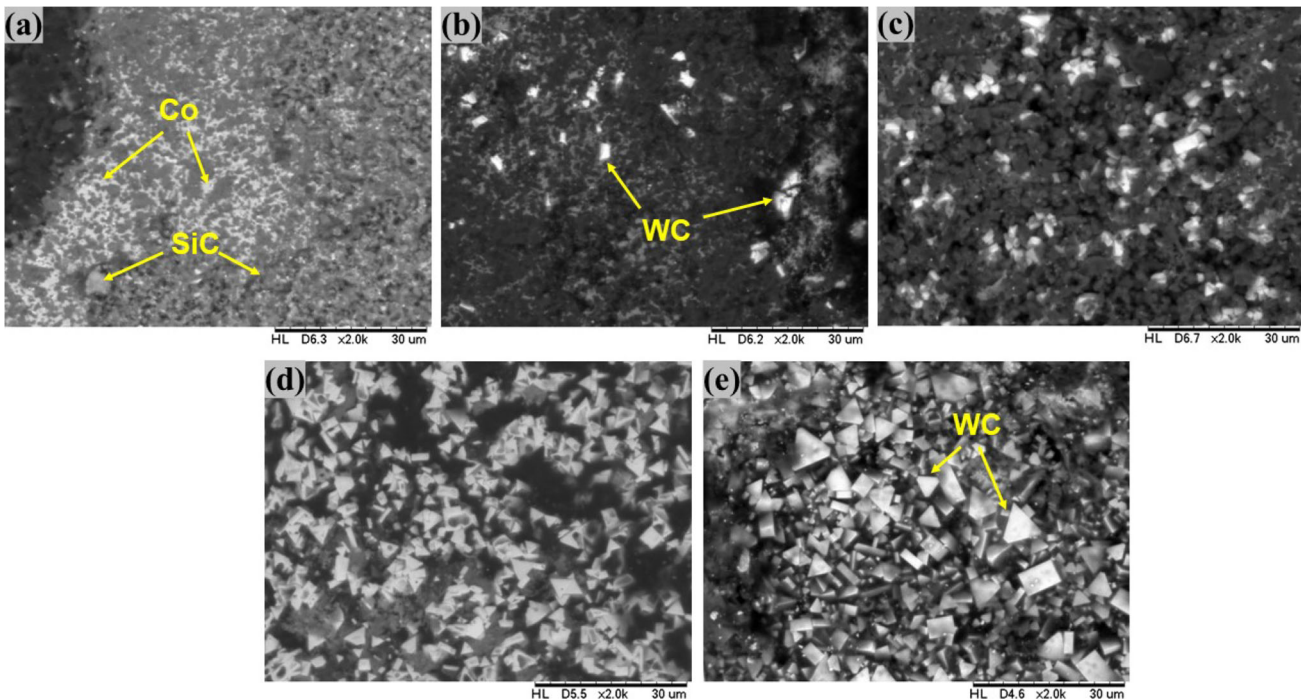


Fig. 6. SEM images of sintered composites x SiC— $(1-x)$ WC—10 wt.% Co for 30 h: (a) $x = 1$, (b) $x = 0.75$, (c) $x = 0.50$, (d) $x = 0.25$, and (e) $x = 0$.

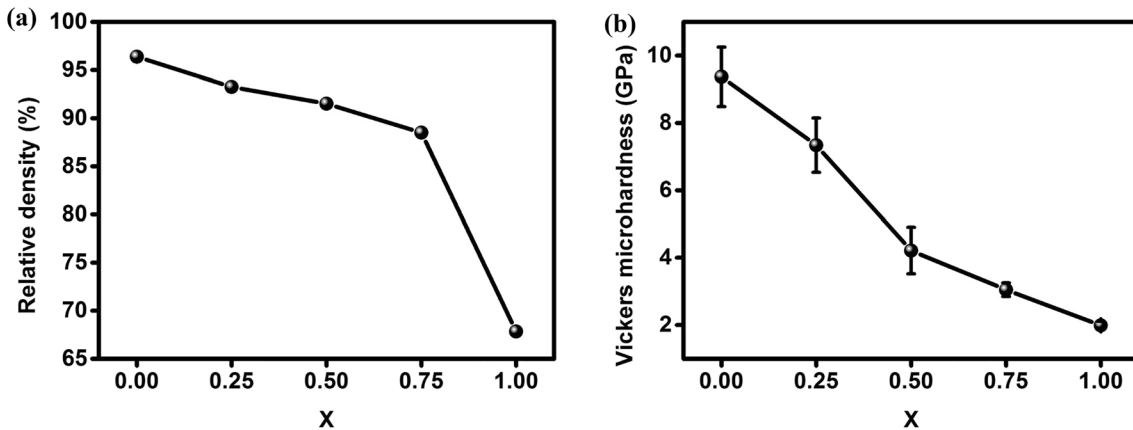


Fig. 7. (a) Relative density and (b) Vickers microhardness of the x SiC— $(1-x)$ WC—10 wt.% Co composites with variation of x (0, 0.25, 0.50, 0.75, 1).

by the Co binder. Thus, the phase dispersion and particle size influence the microstructure, density, and properties (mechanical and tribological) of the composites.

Relative Density and Microhardness of the Sintered Composites

The values of relative density and Vickers microhardness of the sintered composites as a function of the composition are shown in Fig. 7a and b, respectively. Both the relative density and microhardness decreased simultaneously with an increase of SiC content and a decrease in the WC. Such trends are

comparable to the WC-SiC composites.⁴⁷ For $x = 0$ (no presence of SiC), the composite WC-Co exhibited the highest microhardness, about 9.4 GPa, and relative density of 96.37% among all the composites manufactured in this study. As expected, the microhardness increased as the relative density increased.³⁴ With the incorporation of SiC and the reduction of WC ($x = 0.25$), the microhardness (7.43 ± 0.81 GPa) and relative density (93.25%) of the composite started a gradual decay. When the SiC and WC concentrations were equal ($x = 0.5$), the composite exhibited intermediate values of microhardness (4.21 ± 0.69 GPa) and relative density (91.52%). The trend towards a reduction in

microhardness (3.05 ± 0.20 GPa) and relative density (88.51%) with the addition of SiC and decrease of WC was confirmed for the composite with $x = 0.75$. The microhardness (1.99 ± 0.12 GPa) and relative density (67.83%) of the SiC-Co composite ($x = 1$) are significantly lower compared to those of the WC-Co composite ($x = 0$). Both properties decreased sharply with an increase in the content of SiC and the decrease of WC. According to the Hall-Petch relationship, polycrystalline ceramics with greater granulometry have lower hardness values.⁴⁸ According to Leal et al.⁴⁹ the preparation of powder by conventional mixing (mechanical mixing) causes damage to the densification and mechanical properties of composite materials in relation to those processed by HEM. As noted, these properties are strongly influenced by HEM, since the decrease in average particle sizes increases the surface area and significantly improves the sinterability of the composites.

Tribological Behavior of the Composites

The SiC composites, as wear-resistant components used in sliding contact applications, at times are used in environments in which lubricants cannot be available and often suffer high friction losses. In addition, the lubrication of components exposed to wear in high temperatures is difficult in certain work conditions. For this reason, the study of the self-lubrication property of SiC^{50,51} ceramics is important.

The SiC was used as second stage as it holds lubricant properties. In effect, the insertion of SiC can help to increase the wear property in the cemented carbide WC-Co. According to Ref 52, the SiC particles are always added to other materials to increase their tribological properties. For instance, one of the main failures of cutting tools is the rapid increase of the temperature in the interaction area between the cutting tool and the work piece during high-speed cutting operations in (50–300 m/min). Liquid lubrication cannot prevent severe deformation of the machining zone, which leads to tool failure. Recent advances with the addition of solid lubricants decrease the friction heating zone and decrease the energy consumption during high-speed cutting.^{53,54}

The curves for the COF of the sintered composites as a function of time during the sliding wear tests in non-lubricated conditions are shown in Fig. 8. The COF of the composites fluctuated at the beginning of the wear test. After the run-in period, the COF was stabilized. Generally, the average COF for sliding SiC-based ceramics ranges from 0.20 to 0.90 with different test parameters and conditions.⁵⁰ Therefore, the COF of composites with the presence of SiC ($x = 1, 0.75, 0.50$, and 0.25 with $\text{COF} = 0.48 \pm 0.10, 0.88 \pm 0.08, 0.31 \pm 0.04$, and 0.86 ± 0.23 , respectively) are in agreement with the literature. Thus, composites with a low friction coefficient ($x = x = 1$

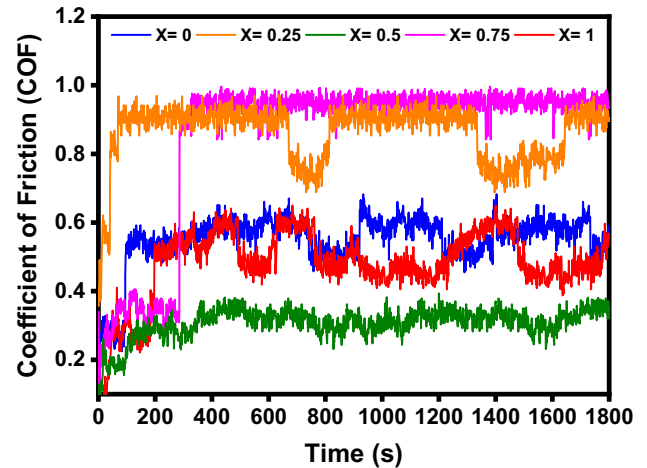


Fig. 8. Evolution of the coefficient of friction of the composites as a function of the sliding time under a 5-N contact load against 1020 steel discs.

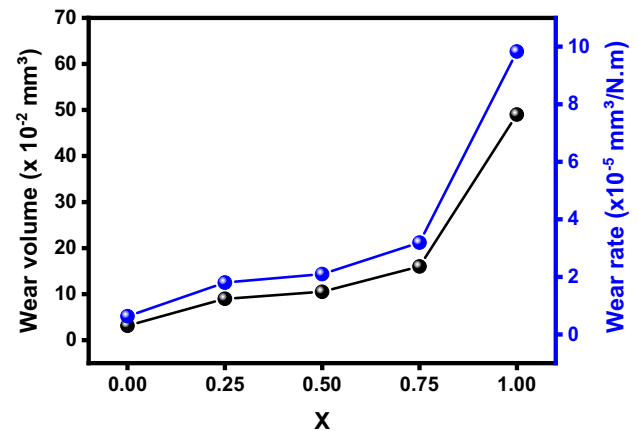


Fig. 9. Tribological behavior: wear volumes and wear rates of composites as a function of composition with a 5-N load against 1020 steel discs.

and 0.50) are beneficial for stress reduction and heat dissipation. While the highest COF values reached by other composites ($x = 0.75$ and 0.25) can be assigned to the detachment of the wear waste which remained stuck between the two sliding bodies (composite and steel disc), has given rise to a third body (layer of transfer) which has significantly affected the friction resistance and the linear variable differential transformer⁵⁵ sensor displacement. Without the presence of SiC ($x = 0$), the mean COF of cemented carbide WC-Co reached 0.55 ± 0.08 .

Changes in the friction response may be correlated with changes in the surface chemistry of the materials as contact occurs. High values of COF result from the effects of mechanical wear, including abrasion or surface fractures,^{56–58} while the formation of hydrated silica or an oxide layer adhered to the interface may be responsible for lower values.^{59–61}

Figure 9 shows the wear volume (V , Eq. 1) and the specific wear rate (K , Eq. 2) estimated for the composites as a function of composition. The increase in wear volume is generally attributed to the increase in fracture for brittle solids.^{62,63} The lowest wear volume ($3.13 \times 10^{-2} \text{ mm}^3$) was obtained for the WC-Co composite ($x = 0$), while the SiC-Co composite ($x = 1$) reached the highest wear volume ($49.0 \times 10^{-2} \text{ mm}^3$), with an increase of at least 15 times in the wear volume. Composites ($x = 0.25, 0.50$, and 0.75) formed within the presence of SiC and WC ceramics exhibited an increase in the wear volume with a decrease in the WC content and a SiC insertion. Previous research has confirmed the reduction in the wear volume with an increase in the content of WC in SiC-WC composites, since the SiC ceramics reinforced with WC has a higher fracture toughness, which led to the reduction of mechanical fracture or grain pulling during sliding in non-lubricated conditions.^{57,60}

In the literature, the wear rates of SiC-based ceramics sintered in the liquid phase have been reported to fluctuate between $10^{-7} \text{ mm}^3/\text{Nm}$ and $10^{-5} \text{ mm}^3/\text{Nm}$ with variable sliding tests in non-lubricated conditions.^{59,61} The wear rates of the composites ranged from $0.63 \times 10^{-5} \text{ mm}^3/\text{Nm}$ to $9.83 \times 10^{-5} \text{ mm}^3/\text{Nm}$. The composites of compositions $x = 0$ (WC-Co) and $x = 1$ (SiC-Co) reached the lowest and highest rates of wear, respectively. The compositions in which the WC and SiC ceramics are present ($x = 0.25, 0.50$, and 0.75) exhibited increasing wear rates with the increase in the WC content and \times reduction of SiC. Other studies have reported a reduction in the wear rate in SiC-WC composites with an increase in WC content.^{57,64} In general, the dense microstructure and greater hardness are beneficial for improving the sliding wear under low load and in non-lubricated conditions.^{65,66}

Surface Roughness Analysis

Profilometry has been a widely used technique for assessing surface imperfections, especially for calculating surface parameters. These analyses allow the characterization of the surface imperfections before and after the wear test.

Figure 10a–j depicts the 3D surface roughness profiles of the specimens before and after the wear test, indicating the progressive surface damage of \times specimens. As a result of wear, one can reasonably and qualitatively assess that the surface roughness profiles have changed to a surface with deeper holes with higher roughness values.

The surface roughness is described by the arithmetic mean value, and is based on the average length between peaks and valleys. The quantitative parameters based on 2D line roughness, such as arithmetic mean deviation of the roughness profile (R_a), and root-mean-square deviation (R_q), as well as the 3D surface profile parameters, such as arithmetic mean height (S_a) and root-mean-square

height (S_q) of the specimens before and after the wear tests were calculated. The definitions of these surface parameters evaluated on the specimens are given in Eqs. (3–6):

$$R_a = \frac{1}{l} \int_0^l |Z(x)| dx \quad (3)$$

$$R_q = \sqrt{\frac{1}{l} \int_0^l |Z^2(x)| dx} \quad (4)$$

$$S_a = \iint_a |Z(x,y)| dx dy \quad (5)$$

$$S_q = \sqrt{\iint_a (Z(x,y))^2 dx dy} \quad (6)$$

where $Z(x)$ corresponds to the height of the profile above mean height value and l refers to the sampling length.

The quantitative parameters based on 2D line roughness, such as R_a , and R_q , as well as the 3D surface profile parameters, S_a and S_q , were evaluated to identify the damage in the specimens. These parameters, before and after the wear tests were calculated according to standards ISO 4287⁶⁷ and ISO 25178,⁶⁸ and are shown in Table I. All the specimens evaluated showed an increase in the surface roughness parameters after the wear tests, which was expected. However, this result only serves as a qualitative parameter, since no correlation was found between these parameters and the composition of the specimens.

CONCLUSION

Composite powders [x SiC–(1– x) WC–10 wt.% Co], with $x = 0, 0.25, 0.50, 0.75$, and 1 , were successfully manufactured by HEM and consolidated by SPS. During HEM, the ceramic particles (SiC, WC) suffered fracture and particle size reduction and were refined and welded in the ductile matrix (Co), positively influencing the densification and mechanical properties of the composites. The average COF of the composites (0.48–0.86) exhibited variations to higher values, correlated to the effects of mechanical wear, while oxide adhered to the interface may be responsible for lower values. The composites exhibited increasing volumes and wear rates with reduced WC content and increased SiC, showing that those with higher relative density and hardness offer greater wear resistance. Tribological tests showed that the composites sintered in this study by SPS proved to be a promising material for applications in components/devices subjected to wear, such as cylinder liners, cutting tools, abrasive machining, valves, etc.

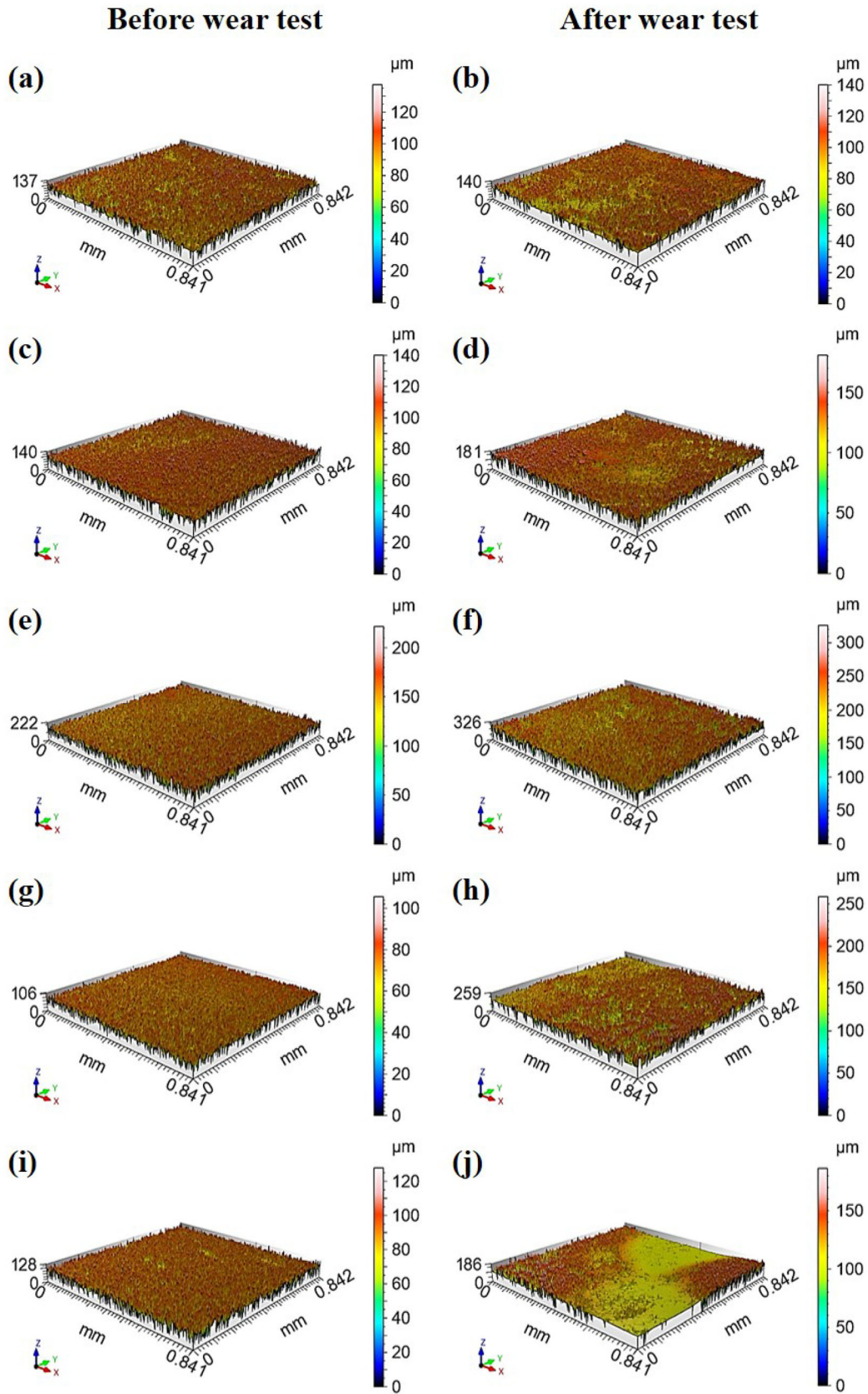


Fig. 10. 3D surface roughness profiles of the specimens before and after the wear test in the following conditions: (a, b) $x = 0$, (c, d) $x = 0.25$, (e, f) $x = 0.5$, (g, h) $x = 0.75$, (i, j) $x = 1$.

Table I. Roughness parameters (μm): linear roughness (Ra and Rq) and surface roughness (Sa and Sq)

Specimens	Before wear test				After wear test			
	Ra	Rq	Sa	Sq	Ra	Rq	Sa	Sq
$x = 0$	12.9	17.7	13.6	18.6	17.7	21.5	16.4	21.4
$x = 0.25$	12.4	16.6	17.7	22.2	20.6	26.1	23.8	29.8
$x = 0.5$	25.7	30.9	27.8	34.1	27.2	37.7	40.8	50.3
$x = 0.75$	13.8	16.4	12.6	15.4	27.7	35.3	27.6	36.6
$x = 1$	13.3	17.4	16.4	20.3	14.8	18.4	17.8	26.2

ACKNOWLEDGEMENTS

The authors would like to acknowledge the support from the Coordenação de Aperfeiçoamento de Pessoal de Nível Superior–Brazil (CAPES)–Finance Code 001. The LAINEZ is acknowledged for supplying the tungsten carbide powder.

FUNDING

General financial support received from CAPES/Brazil. No interference with study design and data analysis.

DATA AVAILABILITY

The raw/processed data required to reproduce these findings cannot be shared at this time as the data also forms part of a continuing study.

CONFLICT OF INTEREST

The authors declare no conflict of interest.

REFERENCES

1. H. Abderrazak, and E.S.B. Hadj Hmi, *in Prop* (Appl, Silicon Carbide (InTech), 2011).
2. B. Ghosh, and S.K. Pradhan, *J. Alloys Compd.* 486, 480 (2009).
3. G. Roewer, U. Herzog, K. Trommer, E. Müller, and S. Frühauf, *in High Perform. Non-Oxide Ceram. I* (Springer Berlin Heidelberg, Berlin, Heidelberg, 2002), pp. 59–135.
4. V. Raman, O.P. Bahl, and U. Dhawan, *J. Mater. Sci.* 30, 2686 (1995).
5. S.K. Sharma, B. Venkata Manoj Kumar, and Y.W. Kim, *Int. J. Refract. Met. Hard Mater.* 68, 166 (2017).
6. S.K. Sharma, B.V.M. Kumar, K.-Y. Lim, Y.-W. Kim, and S.K. Nath, *Ceram. Int.* 40, 6829 (2014).
7. S. Gupta, S.K. Sharma, B.V.M. Kumar, and Y.W. Kim, *Ceram. Int.* 41, 14780 (2015).
8. S.K. Sharma, B.V.M. Kumar, and Y.-W. Kim, *J. Korean Ceram. Soc.* 53, 581 (2016).
9. H. Liu, M.E. Fine, and H.S. Cheng, *J. Am. Ceram. Soc.* 74, 2224 (1991).
10. C. Zishan, L. Hejun, F. Qiangang, C. Yanhui, W. Shaolong, and H. Zibo, *Ceram. Int.* 39, 1765 (2013).
11. B. Guimarães, C.M. Fernandes, D. Figueiredo, M.F. Cerqueira, O. Carvalho, F.S. Silva, and G. Miranda, *Ceram. Int.* 46, 3002 (2020).
12. A. Fazili, M.R. Derakhshandeh, S. Nejadshamsi, L. Nikzad, M. Razavi, and E. Ghasali, *J. Alloys Compd.* 823, 153857 (2020).
13. H.V.S.B. Azevêdo, R.A. Raimundo, D.D.S. Silva, L.M.F. Morais, F.A. Costa, D.A. Macedo, D.G.L. Cavalcante, and U.U. Gomes, *J. Mater. Eng. Perform.* 30, 1504 (2021).
14. X. Li, Y. Liu, W. Wei, M. Du, K. Li, J. Zhou, and K. Fu, *Mater. Des.* 90, 562 (2016).
15. L. An, J. Han, and J. Chen, *J. Univ. Sci. Technol. Beijing. Miner. Metall. Mater.* 13, 174 (2006).
16. Z. Wang, Y. Liu, K. Liu, and B. Wang, *Ceram. Int.* 45, 23658 (2019).
17. P. Siwak, and D. Garbiec, *Trans. Nonferrous Met. Soc. China* 26, 2641 (2016).
18. P.A. Olubambi, K.K. Alaneme, and A. Andrews, *Int. J. Refract. Met. Hard Mater.* 50, 163 (2014).
19. R.M. Genga, G. Akdogan, J.E. Westraadt, and L.A. Cornish, *Int. J. Refract. Met. Hard Mater.* 49, 240 (2015).
20. K.H. Lee, S.I. Cha, B.K. Kim, and S.H. Hong, *Int. J. Refract. Met. Hard Mater.* 24, 109 (2006).
21. H.V.S.B. Azevêdo, R.A. Raimundo, D.D.S. Silva, L.M.F. Morais, D.A. Macedo, D.G.L. Cavalcante, and U.U. Gomes, *Int. J. Refract. Met. Hard Mater.* 94, 105408 (2021).
22. D.M. Hulbert, A. Anders, J. Andersson, E.J. Lavernia, and A.K. Mukherjee, *Ser. Mater.* 60, 835 (2009).
23. D. Hitchcock, R. Livingston, and D. Liebenberg, *J. Appl. Phys* 17(17), 174505 (2015).
24. S. Hocquet, V. Dupont, F. Cambier, F. Ludewig, and N. Vandewalle, *J. Eur. Ceram. Soc.* 40, 2586 (2020).
25. E. Ghasali, R. Yazdani-rad, K. Asadian, and T. Ebadzadeh, *J. Alloys Compd.* 690, 512 (2017).
26. E. Ghasali, H. Nouranian, A. Rahbari, H. Majidian, M. Alizadeh, and T. Ebadzadeh, *Mater. Res.* 19, 1189 (2016).
27. Z.A. Munir, U. Anselmi-Tamburini, and M. Ohyanagi, *J. Mater. Sci.* 41, 763 (2006).
28. C. Suryanarayana, *Prog. Mater. Sci.* 46, 1 (2001).
29. C. Suryanarayana, and N. Al-Aqeeli, *Prog. Mater. Sci.* 58, 383 (2013).
30. N.T. Câmara, R.A. Raimundo, C.S. Lourenço, L.M.F. Morais, D.D.S. Silva, R.M. Gomes, M.A. Morales, D.A. Macedo, U.U. Gomes, and F.A. Costa, *Adv. Powder Technol.* 32, 2950 (2021).
31. M.C.L. Silva, M.M.B. Leite, R.A. Raimundo, G.F. Henriques, S.M. Valcacer, M. Mashhadikarimi, M.A. Morales, and U.U. Gomes, *Ceram. Int.* 48, 19026 (2022).
32. M. Shirani, M. Rahimpour, M. Zakeri, S. Safi, and T. Ebadzadeh, *Ceram. Int.* 43, 14517 (2017).
33. J.F. Guria, A. Bansal, V. Kumar, and B.V. Manoj Kumar, *Ceram. Int.* 48, 12675 (2022).
34. E. Ghasali, T. Ebadzadeh, M. Alizadeh, and M. Razavi, *J. Alloys Compd.* 786, 938 (2019).
35. S. Liu, D.Q. Yi, Y.X. Li, and D. Zou, *Acta Metall. Sin.* 15, 448 (2002).
36. R.A. Raimundo, K.V.A. Santos, C.S. Lourenço, F.A. Costa, M.A. Morales, D.A. Macedo, A.G.P. Silva, and U.U. Gomes, *Ceram. Int.* 47, 677 (2021).
37. C.A. Schneider, W.S. Rasband, and K.W. Eliceiri, *Nat. Methods* 9, 671 (2012).
38. ASTM B962-13: Standard Test Methods for Density of Compacted or Sintered Powder Metallurgy (PM) Products Using Archimedes' Principle. ASTM International (2013).
39. K. Ponhan, K. Tassenberg, D. Weston, K.G.M. Nicholls, and R. Thornton, *Ceram. Int.* 46, 26956 (2020).
40. M.A. Taha, and M.F. Zawrah, *Ceram. Int.* 46, 19519 (2020).

41. ASTM E384-99: Standard Test Method for Microindentation Hardness of Materials. ASTM International (1999).
42. J.F. Archard, *J. Appl. Phys.* 24, 981 (1953).
43. W. Pitschke, H. Hermann, and N. Mattern, *Powder Diffr.* 8, 74 (1993).
44. P. Krishna, and A.R. Verma, *Acta Crystallogr.* 15, 383 (1962).
45. E. A. Owen and D. M. Jones, *IOPScience* 456 (1954).
46. J. Garcia, V. Collado Ciprés, A. Blomqvist, and B. Kaplan, *Int. J. Refract. Met. Hard Mater.* 80, 40 (2019).
47. A. Nino, Y. Nakaibayashi, S. Sugiyama, and H. Taimatsu, *Mater. Trans.* 52, 1641 (2011).
48. R.W. Rice, C.C. Wu, and F. Boichelt, *J. Am. Ceram. Soc.* 77, 2539 (1994).
49. E.A.D. Leal, U.U. Gomes, S.M. Alves, and F.A. Costa, *Int. J. Refract. Met. Hard Mater.* 92, 105275 (2020).
50. W. Zhang, S. Yamashita, and H. Kita, *Mater. Des.* 190, 108528 (2020).
51. W. Zhang, S. Yamashita, and H. Kita, *J. Mater. Res. Technol.* 9, 12880 (2020).
52. W. Zhang, *Curr. Opin. Solid State Mater. Sci.* 26, 101000 (2022).
53. A. Öztürk, K.V. Ezirmik, K. Kazmanlı, M. Ürgen, O.L. Eryılmaz, and A. Erdemir, *Tribol. Int.* 41, 49 (2008).
54. M. Sarkar, and N. Mandal, *Mater. Today Proc.* 66, 3762 (2022).
55. M. Godet, *Wear* 136, 29 (1990).
56. K.H. Zum Gahr, R. Blattner, D.H. Hwang, and K. Pöhlmann, *Wear* 250(1–12), 299–310 (2001).
57. S.K. Sharma, B.V.M. Kumar, and Y.W. Kim, *Ceram. Int.* 41, 3427 (2015).
58. D.C. Cranmer, *J. Mater. Sci.* 20, 2029 (1985).
59. V.S.R. Murthy, H. Kobayashi, S. Tsurekawa, N. Tamari, T. Watanabe, and K. Kato, *Tribol. Int.* 37, 353 (2004).
60. S.K. Sharma, B.V. Manoj Kumar, and Y.W. Kim, *Friction.* 7, 129–142 (2019).
61. P. Andersson, and A. Blomberg, *Wear* 174, 1 (1994).
62. B.M. Kumar, Y.W. Kim, D.S. Lim, and W.S. Seo, *Ceram. Int.* 37(8), 3599–3608 (2011).
63. S.K. Sharma, B.V. Kumar, K.Y. Lim, Y.W. Kim, and S.K. Nath, *Ceram. Int.* 40(5), 6829–6839 (2014).
64. S.K. Sharma, B.V.M. Kumar, B.B. Zugelj, M. Kalin, and Y.W. Kim, *Ceram. Int.* 43, 16827 (2017).
65. I. Gotman, E.Y. Gutmanas, and G. Hunter, *Compr. Biomat. II* 1, 165 (2017).
66. W. Fu, Q.Y. Chen, C. Yang, D.L. Yi, H.L. Yao, H.T. Wang, G.C. Ji, and F. Wang, *Ceram. Int.* 46, 14940 (2020).
67. ISO 4287–02: Geometrical Product Specifications (GPS) – Surface Texture: Profile Method–Terms, Definitions and Surface Texture Parameters (2002).
68. ISO 25178–2: Geometrical Product Specifications (GPS)–Surface Texture: Areal–Part 2: Terms, Definitions and Surface Texture Parameters (2012).

Publisher's Note Springer Nature remains neutral with regard to jurisdictional claims in published maps and institutional affiliations.

Springer Nature or its licensor (e.g. a society or other partner) holds exclusive rights to this article under a publishing agreement with the author(s) or other rightsholder(s); author self-archiving of the accepted manuscript version of this article is solely governed by the terms of such publishing agreement and applicable law.